Weakly bound neutrons and quadrupole response function in the many-body pair correlation of neutron drip line nuclei

2006 J. Phys. G: Nucl. Part. Phys. 32 1105

(http://iopscience.iop.org/0954-3899/32/8/003)

INSTITUTE OF PHYSICS PUBLISHING JOURNAL OF PHYSICS G: NUCLEAR AND PARTICLE PHYSICS

J. Phys. G: Nucl. Part. Phys. **32** (2006) 1105–1119 doi:10.1088/0954-3899/32/8/003

Weakly bound neutrons and quadrupole response function in the many-body pair correlation of neutron drip line nuclei

I Hamamoto[1,2], **H Sagawa**[3] **and Xian-Rong Zhou**[3,4]

[1] Division of Mathematical Physics, Lund Institute of Technology at the University of Lund, Lund, Sweden
[2] The Niels Bohr Institute, Blegdamsvej 17, Copenhagen Ø, DK-2100, Denmark
[3] Center for Mathematical Sciences, University of Aizu, Ikki-machi, Aizu-Wakamatsu, Fukushima 965, Japan
[4] Department of Physics, Xiamen University, Xiamen 361005, People's Republic of China

Received 10 April 2006
Published 30 June 2006
Online at stacks.iop.org/JPhysG/32/1105

Abstract

A simplified model of the Hartree–Fock Bogoliubov (HFB) equation with surface-type or volume-type pairing is solved in coordinate space with the correct asymptotic boundary conditions. By using the resulting HFB wavefunctions, the low-energy quadrupole ($L = 2$) response function is studied for the system with weakly bound s and d neutrons. As the binding energy of the neutrons becomes small or approaches zero, the discrete solutions of the HFB equation disappear. Then, without any further correlation (for example, random phase approximation (RPA) correlation), the threshold quadrupole response becomes broader and moves toward very low excitation energies, while the total strength increases very rapidly. The important role of the continuum character of the upper component $u_{\ell j}(r)$ of the HFB $s_{1/2}$ wavefunction in the increasing strength is pointed out. The large and broad quadrupole response with a very low peak energy is expected for neutron drip line nuclei with $N \approx 56$ and $Z \approx 28$, of which both the neutron $2d_{5/2}$ and $3s_{1/2}$ orbits may be weakly bound in the Hartree–Fock (HF) potential.

(Some figures in this article are in colour only in the electronic version)

1. Introduction

The physics of nuclei far from the β stability line, especially close to the neutron drip line, provides a challenge to the conventional theory of nuclear structure. Weakly bound neutrons with small orbital angular momentum ℓ play a unique role in neutron drip line nuclei, since they have an appreciable probability to be outside the core nucleus and are thereby insensitive to the strength of the potential provided by the well-bound nucleons in the system. Those

neutrons are especially sensitive to the coupling to the nearby continuum of unbound states and are known to be the origin of halo phenomena, change of shell structure, low-energy threshold strength, unique response functions to various external fields. It was also pointed out in [1] that the extended one-particle wavefunctions of lower ℓ orbitals lead to smaller spin-orbit splitting, due to the smaller probability of those particles around the nuclear surface where the spin-orbit potential is effective.

In medium–heavy nuclei the occupancy of low-ℓ weakly bound neutrons will not make a significant contribution to the one-body potential and the many-body pair correlation, partly because the number of particles which can occupy those orbits is a small fraction and partly because they are weakly coupled to the core nucleus. Neglecting the contribution, we have developed a simplified model of HFB [2–4]. In [2, 3] the HFB equation in a simplified model was solved in coordinate space with the correct boundary conditions [5–7], and the many-body pair correlation in neutron drip line nuclei was studied for weakly bound neutrons with various ℓ values. Various aspects of weakly bound $s_{1/2}$ neutrons are especially examined in [3]. In [4] the spin response function is studied for weakly bound $\ell = 1$ neutrons. We have found that as the one-particle binding energy approaches zero the effective pair gap of $s_{1/2}$ neutrons approaches zero and, thus, the possible $s_{1/2}$ occupation probability in the ground state of even–even nuclei may concentrate on the degree of freedom corresponding to the region of very small quasiparticle energy. Then, quadrupole ($L = 2$) response of even–even nuclei may be useful for detecting the low-energy occupation probability. The strength of quadrupole response may be energetically pushed down by the possible coupling to other particle-hole (p-h) excitations, but it is very unlikely that the strength is pushed up. In any case the coupling is expected to be weak for weakly bound low-ℓ neutrons. In order to study the response functions for exciting weakly bound *s* and *d* neutrons by quadrupole operators, we employ the same model as used in [2–4].

A continuum quasiparticle random phase approximation (QRPA) was developed in [8, 9] and applied to calculate the quadrupole response of oxygen isotopes. Since the neutron separation energies of these isotopes are rather large $S_n \sim 4$ MeV, the results did not show a clear sign of the importance of the continuum in the low-energy response when halo neutrons are present in the ground state. In [8, 10] Matsuo *et al* solved the QRPA equation utilizing the exact quasiparticle Green function satisfying the proper outgoing boundary condition for neutrons, while the HFB wavefunctions used in the QRPA were calculated in a finite box with $R_{\max} = 20$ fm. In the case that the upper components of the HFB formalism are continuum functions, their behaviour depends on the size of the finite box, especially outside the nuclear potential. The consequence of the possible dependence of various calculated quantities on the box size must be carefully checked, especially for nuclei in which low-ℓ weakly bound neutrons can be occupied. It should be noticed that the upper components of the HFB wavefunctions obtained in the present paper are accurate also in the case of continuum wavefunctions.

In [8–10], the RRA correlations were taken into account in the study of low-energy 2^+ states in unstable nuclei. The RPA correlations are important for collective excitations of nuclei, in general, shifting the peak energy of isoscalar quadrupole strength lower and at the same time increasing the transition strength in the low-energy region. This result due to the correlation, which is already known in stable nuclei, is found also in neutron-rich oxygen isotopes with the separation energies $S_n \sim 4$ MeV [8, 9]. In this paper, however, we will study the threshold strength in very loosely bound nuclei with the neutron separation energy $S_n < 1$ MeV. In this particular case, it was shown that the low-energy strength is exclusively of the nature of one-particle excitations and the RPA correlations are negligibly small in the continuum RPA calculations without the pairing [11]. It was recently pointed out in [12] that the pairing correlations may increase the RPA correlations even in the loosely bound nucleus

with $S_n = 0.5$ MeV by using a HFB model in which the continuum is discretized in a large box. However, solving QRPA in a finite box might be more riskful than calculating HFB in the same way since in QRPA one must evaluate, for example, the radial integral which contains the product of four continuum wavefunctions (the upper component of HFB wavefunctions). Therefore, we think that it is still an open question how much the RPA correlations will remain in the low-energy threshold strength of very loosely bound nuclei when the proper boundary condition is adopted for the continuum wavefunctions.

Our main aim is to examine general properties of the quadrupole response related to weakly bound low-ℓ neutrons, rather than performing fully self-consistent numerical calculations of HFB+QRPA for specific nuclei. We will focus our attention on the role of the continuum under the many-body pair correlations and study quantitatively the consequence of the continuum wavefunctions of the HFB upper component, especially in the case of the neutron separation energy $S_n < 1$ MeV. To our knowledge these cases have not been systematically studied in the literature. For this end, we adopt a medium heavy mass $A = 84$ and examine the special role of the $3s_{1/2}$ state in the continuum response. This paper is organized as follows. In section 2 we briefly describe our model and present related formulae, while numerical results and discussions are given in section 3. Conclusions are drawn in section 4.

2. Model and formulae

We give a brief summary of our model, which is the same as that used in [2, 3]. We consider the time-reversal invariant and spherically symmetric system with monopole pairing correlation. Taking into account the coupling of neutrons with ℓ and j to the HF central and spin-orbit potentials, $V(r)$ and $V_{so}(r)$, and the pairing field $\Delta(r)$, both of which are given by the well-bound core nucleons, our HFB equation is reduced to the following two-channel coupled equations:

$$\left.\begin{aligned}\left(\frac{\mathrm{d}^2}{\mathrm{d}r^2} - \frac{\ell(\ell+1)}{r^2} + \frac{2m}{\hbar^2}(\lambda + E_{\mathrm{qp}} - V(r) - V_{so}(r))\right) u_{\ell j} - \frac{2m}{\hbar^2}\Delta(r) v_{\ell j} = 0,\\ \left(\frac{\mathrm{d}^2}{\mathrm{d}r^2} - \frac{\ell(\ell+1)}{r^2} + \frac{2m}{\hbar^2}(\lambda - E_{\mathrm{qp}} - V(r) - V_{so}(r))\right) v_{\ell j} + \frac{2m}{\hbar^2}\Delta(r) u_{\ell j} = 0,\end{aligned}\right\} \tag{1}$$

where $u_{\ell j}$ and $v_{\ell j}$ express the upper and lower components of the radial wavefunctions in the HFB approximation, respectively. We take positive quasiparticle energies $E_{\mathrm{qp}} > 0$ and consider bound states $\lambda < 0$. Then, $(\lambda - E_{\mathrm{qp}})$ is always negative, while $(\lambda + E_{\mathrm{qp}})$ can be either negative or positive.

The normalization in the case of $(\lambda + E_{\mathrm{qp}}) < 0$, where E_{qp} expresses a discrete eigenvalue of the HFB equation, is written as

$$\int_0^\infty \mathrm{d}r\,(|u_{\ell j}(E_{\mathrm{qp}}, r)|^2 + |v_{\ell j}(E_{\mathrm{qp}}, r)|^2) = 1, \tag{2}$$

while in the case of $(\lambda + E_{\mathrm{qp}}) > 0$, where the solution of equation (1) exists for any value of E_{qp}, we normalize $u_{\ell j}$ by [2, 5, 7]

$$\int_0^\infty \mathrm{d}r\, u_{\ell j}(E_{\mathrm{qp}}, r) u_{\ell j}(E'_{\mathrm{qp}}, r) = \delta(E_{\mathrm{qp}} - E'_{\mathrm{qp}}). \tag{3}$$

The normalization of the lower component of the radial wavefunction $v_{\ell j}$ in the latter case is determined by equation (3) via the HFB equation (1), and the quantity

$$\int_0^\infty |v_{\ell j}(E_{\mathrm{qp}}, r)|^2\,\mathrm{d}r \qquad \text{where} \quad (\lambda + E_{\mathrm{qp}}) > 0, \tag{4}$$

represents the occupation number probability density per unit energy interval [5].

For simplicity, we replace the HF potential by the Woods–Saxon potential together with the spin-orbit potential, of which the parameters are the standard ones used in β stable nuclei [2, 13]. For the given radius $R = r_0 A^{1/3}$ with $r_0 = 1.27$ fm, the diffuseness $a = 0.67$ fm and the standard strength of spin-orbit potential, we vary the potential strength by changing the depth of the Woods–Saxon potential, $V_{\rm WS}$, so that the corresponding single-particle energy $\varepsilon_{\rm WS}$ is varied. Writing

$$f(r) = \frac{1}{1 + \exp\left(\frac{r-R}{a}\right)}, \tag{5}$$

we perform numerical calculations using the volume-type pairing,

$$\Delta(r) \propto f(r) \tag{6}$$

and also the surface-type pairing,

$$\Delta(r) \propto r \frac{\mathrm{d}f(r)}{\mathrm{d}r}. \tag{7}$$

The averaged strength of the pair field defined by

$$\bar{\Delta} \equiv \frac{\int_0^\infty r^2\,\mathrm{d}r\;\Delta(r) f(r)}{\int_0^\infty r^2\,\mathrm{d}r\;f(r)} \tag{8}$$

is an input of numerical calculations expressing the strength of the pair field. In the present study, we fix the averaged strength of the pair field $\bar{\Delta}$ =1 MeV.

In solving the HFB equation (1) in coordinate space, we use a radial mesh $\Delta r = 0.025$ fm in the neighbourhood of the origin $r = 0$, while $\Delta r = 0.2$ fm is used otherwise. The way of solving the coupled equations (1) is taken from [14]. Solving the HFB equation with the correct asymptotic boundary conditions together with the normalization conditions, (2) and (3), both $u_{\ell j}(E_{\rm qp}, r)$ and $v_{\ell j}(E_{\rm qp}, r)$ wavefunctions are fully independent of the maximum value $R_{\rm max}$ of the actual radial integration as far as the potentials are totally negligible at $r = R_{\rm max}$. In particular, $u_{\ell j}(E_{\rm qp}, r)$ thus obtained does not at all depend on $R_{\rm max}$, even in the case that it is a continuum wavefunction for $(\lambda + E_{\rm qp}) > 0$.

We expect that both the one-body potentials $V(r)$ and $V_{so}(r)$ and the many-body pair-field $\Delta(r)$ come almost exclusively from the well-bound or (weakly bound, but) high-ℓ particles. Thus, in our present work we study the behaviour of weakly bound $s_{1/2}$ and $d_{5/2}$ neutrons in the many-body pair correlation expressed by given $V(r)$, $V_{so}(r)$ and $\Delta(r)$. The importance of the self-consistency was suggested for the pairing correlations in nuclei near the drip line in [12], in which the continuum was discretized in a large box. In [12] the effective pair-gap $\Delta_{\rm eff}$ was defined as the average of the HFB quasiparticle energy weighted with the occupation probabilities below $E_{\rm qp} = 10$ MeV, independent of the sign of $(E_{\rm qp} + \lambda)$. In contrast, in [2, 4] $\Delta_{\rm eff}$ was defined as the lowest HFB quasiparticle energy only for $(E_{\rm qp} + \lambda) < 0$, considering the well-known relation between the pair gap and the (discrete) quasiparticle energies in the BCS approximation. Since in the case of $(\lambda + E_{\rm qp}) > 0$ the HFB quasiparticle spectra are present continuously for $E_{\rm qp} > |\lambda|$, the physical meaning of $\Delta_{\rm eff}$ defined in [12] can be questioned. In order to make a more quantitative argument of the importance of the self-consistent treatment of pair correlation, we need a self-consistent HFB calculation taking into account the continuum effect with proper asymptotic boundary condition [7].

We study the response function of the ground state of even–even nuclei, namely the quasiparticle vacuum, to quadrupole operator $\hat{O}(L = 2) = r^2 Y_{2\mu}$, using the wavefunctions $u_{\ell j}$ and $v_{\ell j}$ obtained by solving equation (1). Denoting the two quasiparticles by i and j, we have three kinds of responses depending on the combination of the signs of $(\lambda + E_i)$ and $(\lambda + E_j)$. (dd): when $(\lambda + E_i) < 0$ and $(\lambda + E_j) < 0$, we obtain the strength

$$B(\omega = E_i + E_j) = |\langle (ij)J^\pi = 2^+ \| \hat{O}(L=2) \| 0^+ \rangle|^2$$
$$= \left| \int_0^{r_{\max}} \mathrm{d}r \langle i \| \hat{O}(L=2) \| j \rangle (u_i(E_i, r) v_j(E_j, r) + u_j(E_j, r) v_i(E_i, r)) \right|^2 \quad (9)$$

at a discrete state with $\omega = E_i + E_j$; (dc): when $(\lambda + E_i) < 0$ and $(\lambda + E_j) > 0$, a continuous spectrum of the strength per unit energy at ω

$$S(\omega = E_i + E_j) = \int \mathrm{d}E_j |\langle (ij)J^\pi = 2^+ \| \hat{O}(L=2) \| 0^+ \rangle|^2 \delta(E_i + E_j - \omega)$$
$$= \left| \int_0^{r_{\max}} \mathrm{d}r \langle i \| \hat{O}(L=2) \| j \rangle (u_i(E_i, r) v_j(E_j, r) + u_j(E_j, r) v_i(E_i, r)) \right|^2, \quad (10)$$

where $E_j > |\lambda|$ is a continuous variable, is obtained; (cc): when $(\lambda + E_i) > 0$ and $(\lambda + E_j) > 0$, the response function per unit energy at ω, which is a continuous spectrum starting at $\omega = 2|\lambda|$, is calculated by using the formula

$$S(\omega) = \int \mathrm{d}E_i \int \mathrm{d}E_j |\langle (ij)J^\pi = 2^+ \| \hat{O}(L=2) \| 0^+ \rangle|^2 \delta(E_i + E_j - \omega)$$
$$= \int_{|\lambda|}^{\omega - |\lambda|} \mathrm{d}E_i \left| \int_0^{r_{\max}} \mathrm{d}r \langle i \| \hat{O}(L=2) \| j \rangle \right.$$
$$\left. \times (u_i(E_i, r) v_j(\omega - E_i, r) + u_j(\omega - E_i, r) v_i(E_i, r)) \right|^2. \quad (11)$$

In the numerical calculations of equations (9), (10) and (11) we use $r_{\max} = 64$ fm. If for $\omega > 2|\lambda|$ both equations (10) and (11) have non-zero contributions, the response of the system is the sum of the two contributions. The difference between the dimension of $B(\omega)$ in (9) and that of $S(\omega)$ in (10) and (11) comes from the fact that the normalizations of $u_{\ell j}$ and $v_{\ell j}$ are different depending on the sign of $(\lambda + E_{\ell j})$.

The non-energy-weighted integrated strength (NEWIS) and energy-weighted integrated strength (EWIS) are defined by

$$m_0(\mathrm{HFB}) = \sum_n B(\omega_n) + \int^{\omega_{\max}} \mathrm{d}\omega S(\omega) \quad (12)$$

and

$$m_1(\mathrm{HFB}) = \sum_n \omega_n B(\omega_n) + \int^{\omega_{\max}} \omega \, \mathrm{d}\omega S(\omega), \quad (13)$$

respectively, where $\omega_{\max} = 10$ MeV is used since we are interested in the low-energy strength. In the above expressions, (12) and (13), the first term on rhs has non-zero contributions only when discrete solutions exist.

We define the occupation probability for $(\lambda + E_{\mathrm{qp}}) > 0$ in the ground state of even–even nuclei by integrating over the relevant energy region

$$v^2_{\mathrm{cont}} \equiv \int_{|\lambda|}^{E_{\max}} \mathrm{d}E_{\mathrm{qp}} \int_0^{r_{\max}} \mathrm{d}r |v_{\ell j}(E_{\mathrm{qp}}, r)|^2 \quad (14)$$

and that for $(\lambda + E_{\mathrm{qp}}) < 0$ by

$$v^2_{\mathrm{disc}} \equiv \int_0^{r_{\max}} \mathrm{d}r \left| v_{\ell j}\left(E^{\mathrm{disc}}_{\mathrm{qp}}, r\right) \right|^2, \quad (15)$$

where we use $E_{\max} = 10$ MeV and $r_{\max} = 64$ fm. The total occupation probability of the one-particle (ℓj) level is the sum of the above two terms,

$$v^2_{\mathrm{total}} = v^2_{\mathrm{disc}} + v^2_{\mathrm{cont}}. \quad (16)$$

The expectation value of mean-square radius for $(\lambda + E_{\rm qp}) < 0$ is defined by

$$\langle r^2\rangle_{\rm disc} \equiv \frac{\int_0^{r_{\rm max}} {\rm d}r\, r^2 \left|v\left(E_{\rm qp}^{\rm disc}, r\right)\right|^2}{v_{\rm disc}^2}, \tag{17}$$

while that for $(\lambda + E_{\rm qp}) > 0$ by

$$\langle r^2\rangle_{\rm cont} \equiv \frac{\int_{|\lambda|}^{E_{\rm max}} {\rm d}E \int_0^{r_{\rm max}} {\rm d}r\, r^2 |v(E,r)|^2}{v_{\rm cont}^2}. \tag{18}$$

Thus, the averaged value is written as

$$\langle r^2\rangle_{\rm total} \equiv \frac{\int_0^{r_{\rm max}} {\rm d}r\, r^2 \left|v\left(E_{\rm qp}^{\rm disc}, r\right)\right|^2 + \int_{|\lambda|}^{E_{\rm max}} {\rm d}E \int_0^{r_{\rm max}} {\rm d}r\, r^2 |v(E,r)|^2}{v_{\rm disc}^2 + v_{\rm cont}^2}. \tag{19}$$

3. Numerical results and discussions

We study HFB solutions for loosely bound $s_{1/2}$, $d_{5/2}$ and $d_{3/2}$ orbits in the potentials with the radius corresponding to $A = 84$ nuclei. This choice of the radius parameter might be realistic since nuclei with $N \approx 56$ and $Z \approx 28$ have the weakly bound neutron $2d_{5/2}$ as well as $3s_{1/2}$ orbits in the mean-field potential. In order to study a systematic trend of the quadrupole response, the depth of the Woods–Saxon potential $V_{\rm WS}$ is adjusted so as to obtain the single-particle energy of the $2d_{5/2}$ orbit varying from $\varepsilon_{\rm WS}(2d_{5/2}) = -10$ MeV to -0.01 MeV. See table 1 for the relation between numerical values of $V_{\rm WS}$ and $\varepsilon_{\rm WS}(2d_{5/2})$. It is noted that the single-particle energy of the $3s_{1/2}$ orbit is more than 2 MeV higher than that of the $2d_{5/2}$ orbit for the potential which gives $\varepsilon_{\rm WS}(2d_{5/2}) = -10$ MeV. In contrast, for weaker potentials producing $\varepsilon_{\rm WS}(2d_{5/2}) > -0.14$ MeV the $3s_{1/2}$ level lies lower than the $2d_{5/2}$ level. Thus both $2d_{5/2}$ and $3s_{1/2}$ orbits are bound in the limit of $\varepsilon_{\rm WS}(2d_{5/2}) \to 0$. The mean square radius of the $3s_{1/2}$ orbit increases rapidly due to the well-known halo nature of $\ell = 0$ orbits. The single-particle energy of the $2d_{3/2}$ orbit is also listed in table 1. The $2d_{3/2}$ state becomes a resonance state for the weaker Woods-Saxon potential which produces $\varepsilon_{\rm WS}(2d_{5/2}) > -2$ MeV, as is listed in table 1. Even in the case of very small binding energies the mean square radii of both $2d_{5/2}$ and $2d_{3/2}$ orbits do not increase so much as those of the $3s_{1/2}$ orbit, due to the presence of centrifugal barriers.

In table 2 the quasiparticle energies $E_{\rm qp}$, the occupation probabilities $v_{\rm disc}^2$ and the mean-square radii obtained in the HFB calculations are tabulated for the $d_{5/2}$, $s_{1/2}$ and $d_{3/2}$ states with discrete $E_{\rm qp}$ values. The HFB equations are solved taking the Fermi energy $\lambda = \varepsilon_{\rm WS}(2d_{5/2})$, while the depth of the Woods–Saxon potential is expressed by the values of $\varepsilon_{\rm WS}(2d_{5/2})$. The discrete $s_{1/2}$ state is obtained for the potentials producing $\lambda = \varepsilon_{\rm WS}(2d_{5/2}) \leqslant -0.3$ MeV, while the discrete $d_{5/2}$ and $d_{3/2}$ states can be found for $\lambda = \varepsilon_{\rm WS}(2d_{5/2}) \leqslant -0.65$ and -3.0 MeV, respectively. Comparing the results in table 2(a) with those in table 2(b), it is seen that for weakly bound orbits the effective gap is larger for the surface-type pairing while for well-bound orbits it is larger for the volume-type pairing, though the difference for a given $\bar{\Delta}$ value is surprisingly small.

In figure 1, we show the quadrupole response $S(\omega)$ as a function of excitation energy ω, which is calculated using the HFB wavefunctions $u_{d5/2}$, $v_{d5/2}$, $u_{s1/2}$ and $v_{s1/2}$ for various values of $\lambda = \varepsilon_{\rm WS}(2d_{5/2})$. Due to the somewhat larger effective gap, the peaks in figure 1(b) obtained by using the surface pairing lie slightly higher than corresponding ones in figure 1(a) with the volume pairing. In general, there are three contributions, (9), (10) and (11), to the quadrupole strength. However, there is no contribution by $B(\omega)$ in (9) in the plotted

Table 1. Mean-square radii of the $2d_{5/2}$, $3s_{1/2}$ and $2d_{3/2}$ orbits in the Woods–Saxon potential, together with the eigenvalues or one-particle resonant energies with widths. The radius for $A = 84$ nuclei is used for the potential, of which the depth is denoted by $V_{\rm WS}$. For $\varepsilon_{\rm WS}(2d_{5/2}) \geqslant -1.5$ MeV one-particle resonant energies of the $2d_{3/2}$ orbit and their widths shown inside the parentheses are obtained from the phase shift analysis.

$\varepsilon_{\rm WS}$ $(2d_{5/2})$ (MeV)	$V_{\rm WS}$ (MeV)	$\langle r^2\rangle_{\rm WS}$ $(2d_{5/2})$ (fm^2)	$\varepsilon_{\rm WS}$ $(3s_{1/2})$ (MeV)	$\langle r^2\rangle_{\rm WS}$ $(3s_{1/2})$ (fm^2)	$\varepsilon_{\rm WS}$ $(2d_{3/2})$ (MeV) (keV)	$\langle r^2\rangle_{\rm WS}$ $(2d_{3/2})$ (fm^2)
−10.0	−54.283	23.43	−7.834	25.56	−6.651	24.52
−5.0	−46.631	27.63	−3.530	33.54	−2.335	31.48
−3.0	−43.235	31.14	−1.948	42.04	−0.734	40.33
−2.0	−41.400	34.15	−1.222	51.06	−0.009	66.04
−1.5	−40.430	36.39	−0.885	59.00	0.303 (37)	
−1.0	−39.408	39.65	−0.574	72.75	0.617 (189)	
−0.8	−38.980	41.49	−0.459	81.66	0.753 (298)	
−0.65	−38.651	43.22	−0.377	90.75	0.862 (407)	
−0.55	−38.428	44.60	−0.325	98.53	0.939 (501)	
−0.5	−38.314	45.39	−0.300	103.20	0.980 (544)	
−0.3	−37.846	49.61	−0.205	129.40	1.156 (833)	
−0.2	−37.602	52.87	−0.162	150.40	1.256 (1035)	
−0.1	−37.352	58.03	−0.122	181.10	1.365 (1276)	
−0.05	−37.222	62.54	−0.103	202.90	1.426 (1446)	
−0.025	−37.155	66.20	−0.094	216.30	1.458 (1530)	
−0.01	−37.116	69.30	−0.089	224.80	1.478 (1583)	

range of the variable $\lambda = \varepsilon_{\rm WS}(2d_{5/2})$, since no HFB discrete solution for the $d_{5/2}$ orbit is obtained for the Woods–Saxon potential which gives $\varepsilon_{\rm WS}(2d_{5/2}) \geqslant -0.5$ MeV. For the potential producing $\lambda = \varepsilon_{\rm WS}(2d_{5/2}) = -0.5$ MeV the response $S(\omega)$ appears as a sharp peak, since the major contribution comes from $S(\omega)$ in (10), namely due to the presence of the HFB discrete solution for the $3s_{1/2}$ orbit where $E_{\rm qp}^{\rm disc}(3s_{1/2})$ is much smaller than $\bar{\Delta}$. For $\lambda = -0.3$, -0.2 and -0.1 MeV the whole contribution comes from $S(\omega)$ in equation (11). In these cases the response $S(\omega)$ starts at $\omega = 2|\lambda|$, which is much smaller than $2\bar{\Delta}$. In particular, the peak energy of the resonance can become very low when weakly bound $s_{1/2}$ neutrons are involved in the excitations. It is seen from figure 1 that as the value of $\lambda = \varepsilon_{\rm WS}(2d_{5/2})$ increases from -0.5 MeV and approaches zero, the quadrupole response function becomes broader and larger and, at the same time, the major strength shifts to the region of smaller ω values, which are indeed much smaller than $2\bar{\Delta} = 2$ MeV. In the case of $\lambda = \varepsilon_{\rm WS}(2d_{5/2}) = -0.1$ MeV, the quadrupole response shows a peculiar two bump structure. In order to understand this behaviour of the response function $S(\omega)$ in equation (11), in figure 2 the integrals

$$\begin{aligned} UR_{\ell j}(E_{\rm qp}) &\equiv \int_0^{r_{\rm max}} r^2\,{\rm d}r(u_{\ell j}(E_{\rm qp}, r))^2 \\ VR_{\ell j}(E_{\rm qp}) &\equiv \int_0^{r_{\rm max}} r^2\,{\rm d}r(v_{\ell j}(E_{\rm qp}, r))^2 \end{aligned} \tag{20}$$

are shown for the $d_{5/2}$ and $s_{1/2}$ orbits as a function of $E_{\rm qp}$, taking the case of the volume-type pairing and $\lambda = \varepsilon_{\rm WS}(2d_{5/2}) = -0.1$ MeV. The value of $r_{\rm max} = 64$ fm is used. Only the dependence of respective integrals, $UR_{\ell j}$ and $VR_{\ell j}$, on $E_{\rm qp}$ should be learned from figure 2, since the absolute magnitude of $UR_{\ell j}$ has no meaning. As seen in the figure, the radial integral $VR_{\ell j}(E_{\rm qp})$ is localized around $E_{\rm qp} = 0.15$ and 0.55 MeV for the $s_{1/2}$ and $d_{5/2}$ orbits,

Table 2. Quasiparticle energies, occupation probabilities and mean-square radii obtained in HFB calculations for the potential with the radius corresponding to $A = 84$ nuclei. The depth of the Woods–Saxon potential is expressed by the values of $\varepsilon_{\rm WS}(2{\rm d}_{5/2})$. The chemical potential is taken to be $\lambda = \varepsilon_{\rm WS}(2{\rm d}_{5/2})$. The volume-type pairing is adopted in (a), while the surface-type pairing is used in (b). See table 1 for the relation between $V_{\rm WS}$ and $\varepsilon_{\rm WS}(2{\rm d}_{5/2})$. Both chemical potentials and quasiparticle energies are expressed in MeV, while mean-square radii in fm^2.

	$1{\rm d}_{5/2}$			$1{\rm s}_{1/2}$			$1{\rm d}_{3/2}$		
$\varepsilon_{\rm WS}(2{\rm d}_{5/2})$	$E_{\rm qp}$	$v^2_{\rm disc}$	$\langle r^2\rangle$	$E_{\rm qp}$	$v^2_{\rm disc}$	r^2	$E_{\rm qp}$	$v^2_{\rm disc}$	$\langle r^2\rangle$
				(a) Volume-type pairing					
−10.0	0.990	0.481	22.97	2.387	0.038	23.13	3.534	0.020	21.89
−5.0	0.880	0.478	26.68	1.685	0.053	27.97	2.831	0.022	25.20
−3.0	0.805	0.474	29.59	1.261	0.069	32.40	2.411	0.022	27.66
−2.0	0.751	0.470	31.91	0.982	0.085	36.65			
−1.0	0.674	0.460	35.70	0.623	0.123	46.09			
−0.8	0.652	0.454	36.83	0.536	0.137	49.89			
−0.65	0.634	0.448	37.82	0.466	0.151	53.84			
−0.55				0.417	0.163	57.34			
−0.5				0.391	0.168	59.48			
−0.3				0.279	0.172	73.05			
				(b) Surface-type pairing					
−10.0	0.942	0.487	23.26	2.354	0.036	22.41	3.519	0.020	21.71
−5.0	0.907	0.487	26.97	1.678	0.056	27.60	2.842	0.027	25.20
−3.0	0.863	0.485	29.85	1.267	0.076	32.33	2.436	0.030	27.86
−2.0	0.824	0.482	32.14	0.996	0.095	36.79			
−1.0	0.758	0.473	35.82	0.644	0.138	46.40			
−0.8	0.738	0.466	36.90	0.558	0.153	50.18			
−0.65				0.488	0.166	54.07			
−0.55				0.438	0.175	57.48			
−0.5				0.412	0.179	59.57			
−0.3				0.292	0.145	72.95			

respectively. On the other hand, the radial integral $UR_{\ell j}(E_{\rm qp})$ shows an oscillating behaviour typical of a scattering state, and the lowest-lying large peak appears around $E_{\rm qp} = 0.1$ and 0.2 MeV for the $1{\rm s}_{1/2}$ and $1{\rm d}_{5/2}$ orbits, respectively. Noting that $S(\omega)$ in (11) contains the pairing factor $(u_i(E_i, r)v_j(\omega - E_i, r) + u_j(\omega - E_i, r)v_i(E_i, r))^2$, it is understood that the bump appearing on the shoulder of the response at $\omega \sim 0.35$ MeV in figure 1(a) is due to the contributions by the peak of $VR_{s1/2}$ at $E_{\rm qp} = 0.15$ MeV together with that of $UR_{\rm d5/2}$ around $E_{\rm qp} = 0.2$ MeV. On the other hand, the peak at $\omega \sim 0.65$ MeV in figure 1(a) comes from the peak of $VR_{\rm d5/2}$ at $E_{\rm qp} = 0.55$ MeV together with that of $UR_{s1/2}$ around $E_{\rm qp} = 0.1$ MeV.

As far as discrete solutions exist in the HFB equation, the (dd) contribution in (9) is dominant in the total transition strength. Then, the major part of the response appears at the excitation energy of the sum of two quasiparticle energies, $\omega = E_i + E_j$. On the other hand, when the discrete solutions disappear for both i and j orbits, the response coming from the (cc) contribution in (11) has, in general, no longer one-peak structure. This is because the peak energies of $UR_{\ell j}(E_{\rm qp})$ and $VR_{\ell j}(E_{\rm qp})$ are different for $(\lambda + E_{\rm qp}) > 0$, as shown in figure 2. For weakly bound low-ℓ orbits the peak energy of $VR_{\ell j}(E_{\rm qp})$ becomes larger than the energy of the lowest-lying large peak of $UR_{\ell j}(E_{\rm qp})$, as $(\lambda + E_{\rm qp})$ starts to increase from zero. Furthermore, the difference between the peak energies in $VR_{\ell j}$ and $UR_{\ell j}$ depends on orbits

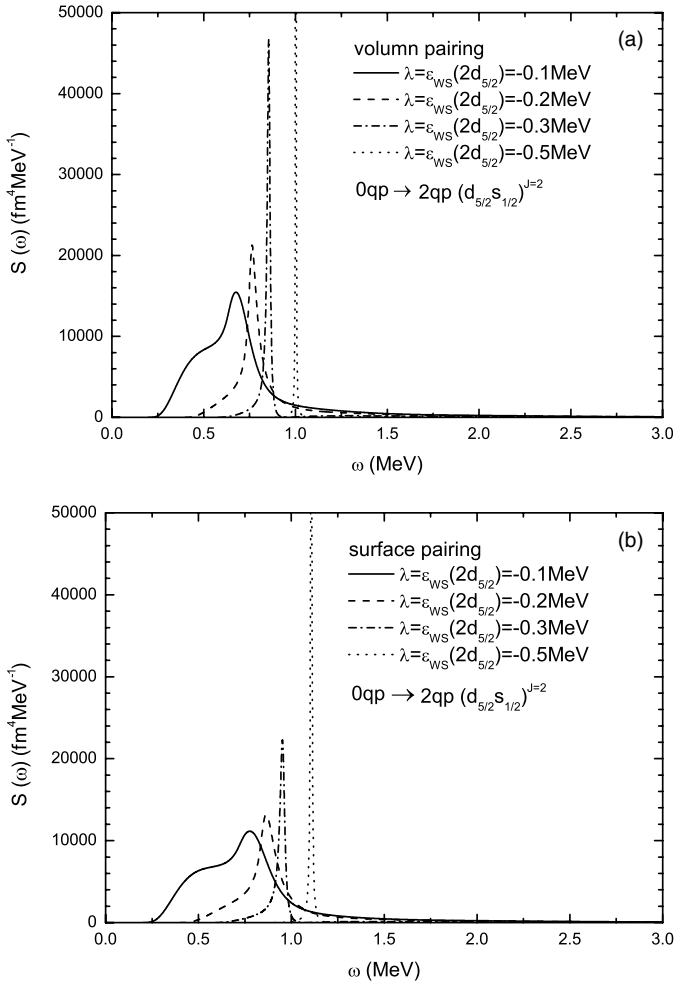

Figure 1. Quadrupole response $S(\omega)$ as a function of excitation energy ω, which is calculated using the HFB wavefunctions, $u_{\mathrm{d5/2}}$, $v_{\mathrm{d5/2}}$, $u_{\mathrm{s1/2}}$ and $v_{\mathrm{s1/2}}$, for the radius of the potential corresponding to $A = 84$ nuclei and various values of $\lambda = \varepsilon_{\mathrm{WS}}(2\mathrm{d}_{5/2})$. The depth of the Woods–Saxon potential is adjusted so as to give respective eigenvalues of $\varepsilon_{\mathrm{WS}}(2\mathrm{d}_{5/2})$. The plotted quantity expresses the sum of two contributions of $S(\omega)$ in equations (10) and (11) for $\lambda = -0.5$ MeV, while it is $S(\omega)$ in equation (11) for $\lambda = -0.3, -0.2$ and -0.1 MeV. The contribution in equation (9) is absent in the range of the present parameters. The volume-type pairing is used in (a), while the surface-type pairing in (b). See the text for details.

(ℓj). As a result of these, the two-bump structure can appear in the response, as seen in the case of $\lambda = \varepsilon_{\mathrm{WS}}(2\mathrm{d}_{5/2}) = -0.1$ MeV in figure 1. It is noted that in the BCS approximation the only contribution to the response is the type of $B(\omega)$ in equation (9), namely the relevant values of E_{qp} are discrete which are common to U and V defined in (21). Therefore, neither continuous spectra nor a two-bump shape appear in the response.

In table 3 we list the calculated HFB integrated strengths as a function of the potential strength which is denoted by the values of $\varepsilon_{\mathrm{WS}}(2\mathrm{d}_{5/2})$. The peak energy E_x tabulated in table 3 is the sum of the two quasiparticle energies when the (dd) contribution is dominant, otherwise it expresses the peak energy of the response. The quadrupole response from the ground state

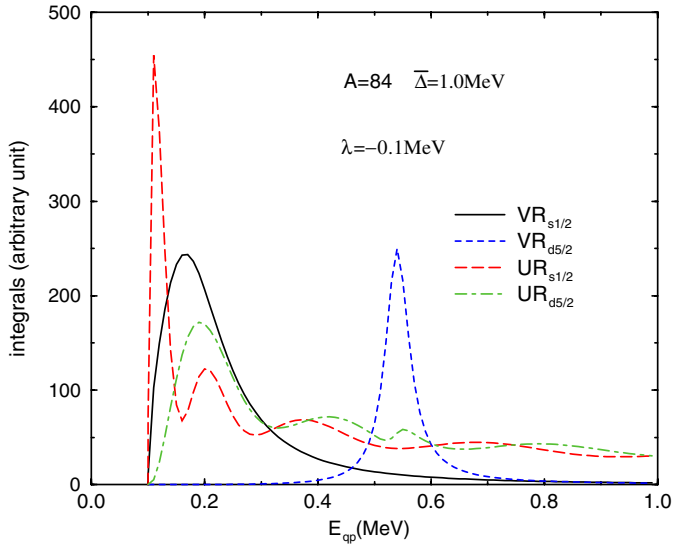

Figure 2. The integrals in (20) for $d_{5/2}$ and $s_{1/2}$ orbits expressed in arbitrary units as a function of $E_{\rm qp}$. Only the dependence of respective integrals on $E_{\rm qp}$ should be learned from the figure. The Fermi level is placed at $\lambda = -0.1$ MeV, while the potential depth $V_{\rm WS}$ is adjusted to produce $\varepsilon_{\rm WS}(2d_{5/2}) = -0.1$ MeV. The volume-type pairing is used in the calculations. See the text for details.

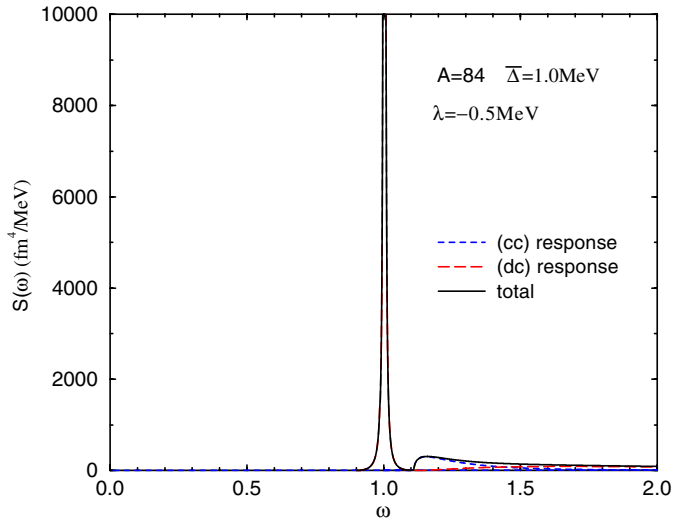

Figure 3. Quadrupole response $S(\omega)$ as a function of excitation energy ω, which is calculated using the HFB wavefunctions $u_{d5/2}$, $v_{d5/2}$, $u_{s1/2}$ and $v_{s1/2}$ for $\lambda = \varepsilon_{\rm WS}(2d_{5/2}) = -0.5$ MeV in $A = 84$ nuclei. The (dd) contribution in equation (9) is absent for the present parameters. The solid curve expresses the sum of two contributions of $S(\omega)$ in equations (10) and (11). The volume-type pairing is used in the calculations. See the text for details.

to the two-quasiparticle (2qp) state $(d_{5/2}s_{1/2})^{J=2}$ is calculated up to the excitation energy $\omega_{\rm max} = 10$ MeV. The three kinds of contributions to the NEWIS m_0 and to the EWIS m_1 are

Table 3. Peak energies E_x, NEWIS m_0 and EWIS m_1 of the HFB quadrupole response of the ground state of even–even nuclei to the 2qp excited states $(d_{5/2}s_{1/2})^{J=2}$. The radius of the potential corresponds to $A = 84$ nuclei, while the depth of the Woods–Saxon potential is expressed by the values of $\varepsilon_{\rm WS}(2d_{5/2})$. The chemical potential is taken to be $\lambda = \varepsilon_{\rm WS}(2d_{5/2})$. The volume-type pairing is used for (a), while the surface-type pairing is adopted for (b). The integrated strengths are obtained by integrating up to $\omega = 10$ MeV. The contributions to the integrated strengths from two discrete qp states (dd), one discrete and one continuum qp states (dc) and two continuum qp states (cc) are shown separately. Both chemical potentials and peak energies are expressed in MeV, NEWIS(m_0) in fm^2, and EWIS(m_1) in fm^2 MeV.

$\varepsilon_{\rm WS}(2d_{5/2})$	E_x	m_0(dd)	m_1(dd)	m_0(dc)	m_1(dc)	m_0(cc)	m_1(cc)
			(a) Volume-type pairing				
−10.0	3.377	168.60	569.35	0.0	0.0	–	–
−5.0	2.565	259.38	665.30	7.44	61.89	–	–
−3.0	2.066	357.85	739.31	15.81	115.30	0.01	0.11
−2.0	1.733	461.64	800.01	25.72	164.79	0.13	1.03
−1.0	1.297	707.18	917.21	73.91	323.24	1.86	11.03
−0.8	1.188	808.27	960.23	109.98	408.86	3.80	20.25
−0.65	1.082	914.28	989.25	160.43	508.76	7.24	34.51
−0.55	1.036	–	–	1180.5	1559.0	76.9	179.4
−0.5	1.002	–	–	1257.4	1618.9	102.7	214.8
−0.3	0.854	–	–	–	–	2169.88	2567.80
−0.2	0.764	–	–	–	–	3160.60	3307.60
−0.1	0.676	–	–	–	–	5823.40	4807.70
			(b) Surface-type pairing				
−10.0	3.296	167.45	551.92	0.0	0.0	–	–
−5.0	2.585	264.69	683.95	11.74	98.35	–	–
−3.0	2.130	369.64	784.75	25.73	190.11	0.02	0.14
−2.0	1.820	480.31	874.16	40.44	265.04	0.24	1.83
−1.0	1.402	736.56	1032.7	99.20	459.19	3.52	21.14
−0.8	1.296	839.45	1087.9	150.01	541.08	7.13	38.71
−0.65	1.207	–	–	1098.2	1681.4	38.44	128.22
−0.55	1.142	–	–	1215.8	1775.8	81.31	217.14
−0.5	1.110	–	–	1280.9	1819.5	129.91	304.73
−0.3	0.952	–	–	1327.5	1580.9	982.5	1426.8
−0.2	0.864	–	–	–	–	3111.09	3581.21
−0.1	0.776	–	–	–	–	5426.40	4940.00

tabulated. In the case that the (dd) contribution exists, it dominates in the integrated strengths, while the (dc) contribution increases rapidly as the potential strength becomes weaker, and the (cc) contribution is negligible. When the discrete solution of the $d_{5/2}$ orbit disappears, the (dc) contribution suddenly absorbs the major part of the integrated strength and the (cc) contribution increases substantially, though the latter is still at most 10% of the total NEWIS value. As an example, the two contributions (10) and (11) are plotted in figure 3, taking the volume-type pairing and $\lambda = \varepsilon_{\rm WS}(2d_{5/2}) = -0.5$ MeV. A sharp peak at $\hbar\omega = 1.0$ MeV is due to the (dc) response, while the (cc) contribution rises just above $\hbar\omega = 1.1$ MeV. For $\lambda \geqslant -0.3$ MeV, we have only the (cc) contributions and the integrated values increase very rapidly for $|\lambda| \to 0$. For reference, in table 4 we show also the integrated values obtained in the BCS approximation. They are estimated using the usual BCS formulae with the pair-gap $\Delta = 1$ MeV and one-particle eigenenergy $\varepsilon_{\rm WS}(\ell j)$ in the Woods–Saxon potentials used for respective HFB calculations. The BCS quasiparticle energy $E_{\rm qp}$ and the pairing U and V

Table 4. Excitation energies E_x, NEWIS m_0 and EWIS m_1 of the BCS quadrupole response of the ground state of even–even nuclei to the 2qp excited states $(2d_{5/2}3s_{1/2})^{J=2}$ and $(2d_{5/2}2d_{3/2})^{J=2}$. The radius of the potential corresponds to $A = 84$ nuclei, while the depth of the Woods–Saxon potential is expressed by the values of $\varepsilon_{\rm WS}(2d_{5/2})$. The chemical potential is taken to be $\lambda = \varepsilon_{\rm WS}(2d_{5/2})$. Both chemical potentials and peak energies are expressed in MeV, NEWIS(m_0) in fm^2, and EWIS(m_1) in fm^2 MeV.

$\varepsilon_{\rm WS}(2d_{5/2})$	$3s_{1/2}$			$2d_{3/2}$		
	E_x	m_0	m_1	E_x	m_0	m_1
−10.0	3.386	182.28	617.15	4.495	49.93	224.44
−5.0	2.778	303.91	844.23	3.846	78.08	300.33
−3.0	2.451	450.45	1104.26	3.477	110.85	385.41
−2.0	2.267	614.45	1392.96	3.228	148.71	480.04
−1.0	2.087	1009.22	2106.20			
−0.8	2.057	1147.33	2359.53			
−0.65	2.037	1314.89	2677.90			
−0.55	2.025	1458.79	2954.05			
−0.5	2.020	1545.60	3121.81			
−0.3	2.005	2064.14	4137.57			
−0.2	2.001	2537.88	5077.59			
−0.1	2.0	3414.54	6829.91			

factors are given by

$$E_{\rm qp} = \sqrt{(\varepsilon_{\rm WS} - \lambda)^2 + \Delta^2},$$
$$U = \frac{1}{\sqrt{2}}\left(1 + \frac{\varepsilon_{\rm WS} - \lambda}{E_{\rm qp}}\right)^{1/2}, \tag{21}$$
$$V = \frac{1}{\sqrt{2}}\left(1 - \frac{\varepsilon_{\rm WS} - \lambda}{E_{\rm qp}}\right)^{1/2}.$$

Note that the BCS occupation and unoccupation amplitudes, V and U, are just numbers and do not depend on r. The 2qp excitation energy, NEWIS m_0 and EWIS m_1 in the BCS approximation are tabulated in table 4, taking $\lambda = \varepsilon_{\rm WS}(2d_{5/2})$. The NEWIS values in the HFB and BCS approximations are compared in figure 4 as a function of $\lambda = \varepsilon_{\rm WS}(2d_{5/2})$. There is a little difference between the NEWIS values obtained from the two HFB calculations. The integrated strengths of BCS are larger than those of HFB below $\lambda = -0.3$ MeV for both volume-type and surface-type pairing . This difference can be understood by examining the U and V factors in the quadrupole response. The response in the BCS approximation has a combination of U and V factors which becomes

$$\left(U_{2d_{5/2}}V_{3s_{1/2}} + V_{2d_{5/2}}U_{3s_{1/2}}\right)^2 = \frac{1}{2}\left(1 + \frac{\Delta}{\sqrt{(\varepsilon_{\rm WS}(2d_{5/2}) - \varepsilon_{\rm WS}(3s_{1/2}))^2 + \Delta^2}}\right), \tag{22}$$

where $\lambda = \varepsilon_{\rm WS}(2d_{5/2})$ is used. The NEWIS in the BCS approximation, m_0(BCS), increases strongly as $\lambda = \varepsilon_{\rm WS}(2d_{5/2})$ increases from −5 MeV, due to not only the strongly increasing mean square radius of the $3s_{1/2}$ state but also the decreasing energy difference $\varepsilon_{\rm WS}(2d_{5/2}) - \varepsilon_{\rm WS}(3s_{1/2})$, which makes the relevant BCS pairing factor $\left|U_{2p_{3/2}}V_{2p_{1/2}} + V_{2p_{3/2}}U_{2p_{1/2}}\right|$ closer to unity. The NEWIS obtained from the HFB calculation, m_0(HFB), are in general somewhat smaller than that of BCS since the mean square radius of the $s_{1/2}$ state is smaller than that

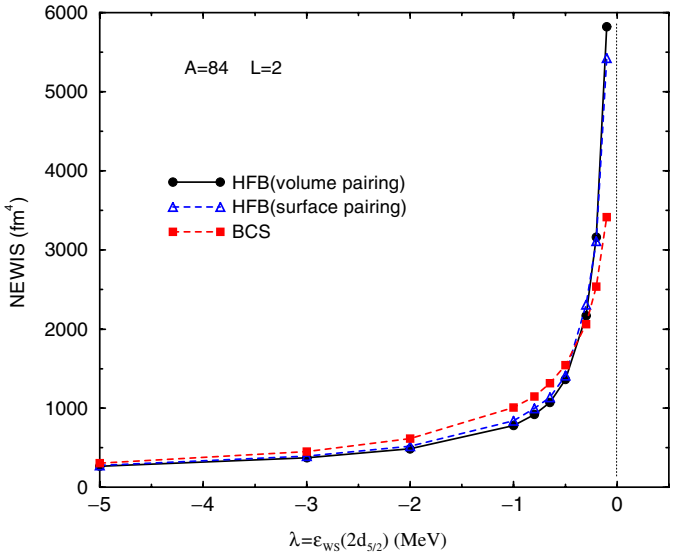

Figure 4. The NEWIS of low-energy (summed for $\omega \leqslant 10$ MeV) quadrupole excitations from the ground state to the 2qp $(d_{5/2}s_{1/2})^{J=2}$ state in the HFB and BCS approximations as a function of $\lambda = \varepsilon_{WS}(2d_{5/2})$. The radius of the Woods–Saxon potential corresponds to $A = 84$ nuclei, while the depth of the potential is adjusted so as to give respective eigenvalues of $\varepsilon_{WS}(2d_{5/2})$. See the text for details.

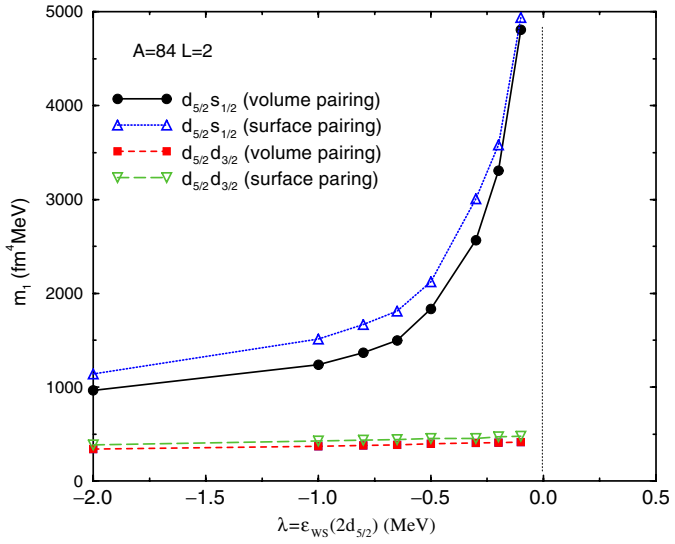

Figure 5. Comparison between the EWIS of low-energy (summed for $\omega \leqslant 10$ MeV) quadrupole excitations from the ground to the 2qp $(d_{5/2}s_{1/2})^{J=2}$ and $(d_{5/2}d_{3/2})^{J=2}$ states in the HFB model as a function of $\lambda = \varepsilon_{WS}(2d_{5/2})$. The radius of the Woods–Saxon potential corresponds to $A = 84$ nuclei, while the depth of the potential is adjusted so as to produce respective eigenvalues of $\varepsilon_{WS}(2d_{5/2})$. See the text for details.

of BCS. Now, in the case of $\lambda > -0.3$ MeV, the two single-particle energies $\varepsilon_{WS}(2d_{5/2})$ and $\varepsilon_{WS}(3s_{1/2})$ are almost degenerate so that the factor $\left|U_{2d_{5/2}}V_{3s_{1/2}} + V_{2d_{5/2}}U_{3s_{1/2}}\right|$ is almost equal to

unity in the BCS approximation. Therefore, the quadrupole response is essentially determined by the matrix element $\langle 2d_{5/2}|r^2|3s_{1/2}\rangle$ with the Woods–Saxon wavefunctions. On the other hand, in the HFB model, the u and v factors are radial dependent and the radial integral of the $(u_{d5/2}v_{s1/2} + v_{d5/2}u_{s1/2})$ factor is somewhat smaller than the corresponding quantity in the BCS approximation. Moreover, the mean-square radii of HFB wavefunctions are appreciably smaller than those of wavefunctions in corresponding Woods–Saxon potentials. Thus, one may expect that the NEWIS values of HFB are in general smaller than those of BCS. However, when for $\lambda > -0.3$ MeV the continuum nature of $u_{s1/2}(r)$ starts to play a dominant role in the response, the HFB integrated strengths become larger than those of BCS. In the case of $\lambda = -0.1$ MeV, m_0(HFB) is 70% larger than m_0(BCS). This large enhancement is entirely due to the feature unique in the continuum wavefunction $u_{s1/2}(r)$ of the HFB model. In contrast, the quasiparticle wavefunctions in the BCS approximation are bound-state wavefunctions as far as the corresponding orbits in the Woods–Saxon potential are bound orbits.

The values of EWIS, m_1, for the 2qp excitations to $(d_{5/2}s_{1/2})^{J=2}$ and $(d_{5/2}d_{3/2})^{J=2}$ are compared in figure 5. Due to the halo nature of the $s_{1/2}$ state, m_1 of the $(d_{5/2}s_{1/2})^{J=2}$ excitation increases very rapidly as λ approaches zero, while m_1 of the $(d_{5/2}d_{3/2})^{J=2}$ excitation stays almost constant. This result is remarkable when one notices that $\varepsilon_{WS}(3s_{1/2}) < 0$ for $\lambda = \varepsilon_{WS}(2d_{5/2}) < 0$, while $\varepsilon_{WS}(2d_{3/2}) > 0$ for $\lambda = \varepsilon_{WS}(2d_{5/2}) > -2$ MeV. Thus, it is seen that the enhancement of the low-energy strength occurs only when weakly bound low-ℓ neutrons are involved in the quasiparticle excitations. Due to the somewhat larger effective gap the m_1 value of the $(d_{5/2}s_{1/2})^{J=2}$ excitation for the surface-type pairing is constantly larger than that for the volume-type pairing. The same effect can be also seen in the m_1 values of the $(d_{5/2}d_{3/2})^{J=2}$ excitation while the difference is small.

Since our system is a bound system, the lower components $v_{\ell j}$ of the HFB radial wavefunctions are always bound-state wavefunctions, while the upper components $u_{\ell j}$ become continuum wavefunctions in the case of $(\lambda + E_{qp}) > 0$. The orthogonality (3) of those continuum $u_{\ell j}(E_{qp}, r)$ functions, for example, can be numerically obtained, only when the radial integral is carried out to infinity. To perform such a numerical integration is practically impossible. Therefore, it is not easy to make a reliable numerical estimate of the response to one-particle operators, which contains a factor of $u_{\ell j}u_{\ell' j'}$ when none of $u_{\ell j}$ and $u_{\ell' j'}$ are bound-state wavefunctions. The quadrupole response, which is studied in the present work, contains the pairing factor $(u_{d_{5/2}}v_{s_{1/2}} + v_{d_{5/2}}u_{s_{1/2}})$, where $v_{\ell j}(E_{qp}, r)$ are always bound-state wavefunctions. Therefore, the quadrupole response may be reliably estimated. We have checked the r_{max} dependence of the numerical values of $S(\omega)$, m_0(HFB) and m_1(HFB), which are given in the present paper, and confirmed that our values are reliable.

In the drip line nuclei in which a discrete solution is absent and $u_{\ell j}(r)$ becomes a continuum wavefunction, we have shown how drastically the quadrupole response changes without any possible RPA correlation. In the self-consistent HF+RPA calculation in the absence of pair correlation it is found [11] that the RPA correlation is very small in the low-energy quadrupole strength just above the threshold in neutron drip line nuclei. On the other hand, it was pointed out recently in [12] that the pairing correlations may increase the RPA correlations even in the loosely bound nuclei using a HFB+QRPA model with the discretized continuum effect in a large box. It remains to see how much the RPA correlation will be effective in the very low-lying threshold strength in the presence of pair correlation when the proper boundary condition is adopted for the continuum wavefunctions. Experimental evidence for the threshold strength may be obtained in proton inelastic scattering or α inelastic scattering experiments with inverse kinematics which will be feasible in future RIB experiments.

4. Conclusions

Using the surface-type and volume-type pairing, we have studied the properties of weakly bound s and d neutrons and the related quadrupole response functions in even–even nuclei, solving a simplified model of the HFB equation in coordinate space with the correct asymptotic boundary conditions. When the binding energies of both $d_{5/2}$ and $s_{1/2}$ neutrons approach zero, we have shown that the peak energy of the quadrupole response becomes drastically lower and the width gets broader, while the total strength increases dramatically without including any RPA correlation. This unique feature of the quadrupole response obtained from HFB will play an important role in low-energy quadrupole excitations in unstable nuclei. Compared with the results in the BCS approximation, the continuum 2qp excitation involving weakly bound $s_{1/2}$ neutrons enhances substantially the NEWIS value. This is particularly interesting, because due to the strong continuum effect the quadrupole response of HFB gives more strength than that of the standard BCS, in spite of the fact that the increase of the HFB mean-square radius is appreciably smaller than that of the mean-field calculations without pair correlations. The excitation of 2qp states without $s_{1/2}$ neutrons shows little enhancement in the quadrupole response. It would be interesting to observe the low-lying quadrupole strength in spherical nuclei with $N \approx 56$ and $Z \approx 28$ in which both $2d_{5/2}$ and $3s_{1/2}$ neutrons are expected to be weakly bound.

Though in the present work we have used a simplified model taking into account neither the self-consistency nor many-particle many-hole states, we believe we have pointed out the important and interesting properties of quadrupole response in connection with the presence of weakly bound low-ℓ neutrons. The properties are strictly related to the continuum character of the upper component of the HFB wavefunctions. It remains to check also how much the RPA correlation in the presence of pair correlation changes the quadrupole threshold strength in the very low-energy region of weakly bound nuclei.

Acknowledgments

This work is supported in part by the Japanese Ministry of Education, Culture, Sports, Science and Technology by Grant-in-Aid for Scientific Research under the program number (C(2)) 16540259. One of the authors (IH) is thankful to Kungliga Fysiografiska Sällskapet i Lund for a financial support for her research project.

References

[1] Hamamoto I, Lukyanov S and Zhang X Z 2001 *Nucl. Phys.* A **683** 255
[2] Hamamoto I and Mottelson B R 2003 *Phys. Rev.* C **68** 034312
[3] Hamamoto I and Mottelson B R 2004 *Phys. Rev.* C **69** 064302
[4] Hamamoto I and Sagawa H 2004 *Phys. Rev.* C **70** 034317
[5] Bulgac A 1980 No. FT-194-1980, Institute of Atomic Physics, Bucharest, *Preprint* nucl-th/9907088
[6] Belyaev S T, Smirnov A V, Tolokonnikov S V and Fayans S A 1987 *Yad. Fiz.* **45** 1263
[7] Grasso M, Sandulescu N, Van Giai Nguyen and Liotta R J 2001 *Phys. Rev.* C **64** 064321
[8] Matsuo M 2001 *Nucl. Phys.* A **696** 371
[9] Khan E, Sandulescu N, Grasso M and Van Giai Nguyen 2002 *Phys. Rev.* C **66** 024309
[10] Matsuo M, Mizuyama K and Serizawa Y 2005 *Phys. Rev.* C **71** 064326
[11] Hamamoto I, Sagawa H and Zhang X Z 1997 *Phys. Rev.* C **55** 2361
[12] Yamagami M 2005 *Phys. Rev.* C **72** 064308
[13] Bohr A and Mottelson B R 1969 *Nuclear Structure* vol I (Reading, MA: Benjamin)
[14] Tamura T 1965 *Rev. Mod. Phys.* **37** 679
Tamura T 1967 ORNL-4152, UC-32 Mathematics and Computers (Oak Ridge National Laboratory, USA)